

Realization of room temperature polaritonic vortex in momentum space with hybrid Perovskite metasurface

Nguyen Ha My Dang,¹ Simone Zanotti,² Emmanuel Drouard,¹ Céline Chevalier,¹ Gaëlle Trippé-Allard,³ Mohamed Amara,¹ Emmanuelle Deleporte,³ Vincenzo Ardiszone,⁴ Daniele Sanvitto,⁴ Lucio Claudio Andreani,² Christian Seassal,¹ Dario Gerace,² and Hai Son Nguyen^{1,5, a)}

¹*Univ Lyon, Ecole Centrale de Lyon, CNRS, INSA Lyon, Université Claude Bernard Lyon 1, CPE Lyon, CNRS, INL, UMR5270, 69130 Ecully, France*

²*Dipartimento di Fisica, Università di Pavia, via Bassi 6, I-27100 Pavia, Italy*

³*Université Paris-Saclay, ENS Paris-Saclay, CNRS, CentraleSupélec, LuMIn, Gif-sur-Yvette, France*

⁴*CNR Nanotec, Institute of Nanotechnology, via Monteroni, 73100, Lecce*

⁵*IUF, Université de France*

(Dated: 1 November 2021)

Exciton-polaritons are mixed light-matter excitations that result from the strong coupling regime between an active excitonic material and photonic resonances. Harnessing these hybrid excitations provides a rich playground to explore fascinating fundamental features, such as out-of-equilibrium Bose-Einstein condensation and quantum fluids of light, as well as novel mechanisms to be exploited in optoelectronic devices. Here, we investigate experimentally the formation of exciton-polaritons arising from the mixing between hybrid inorganic-organic perovskite excitons and an optical Bound state In a Continuum (BIC) of a subwavelength-scale metasurface, at room temperature. These polaritonic eigenmodes, hereby called polariton BICs (pol-BICs) are revealed in both reflectivity, resonant scattering, and photoluminescence measurements. Although pol-BICs only exhibit a finite quality factor that is bounded by the non-radiative losses of the excitonic component, they fully inherit BIC peculiar features: a full uncoupling from the radiative continuum in the vertical direction, which is associated to a locally vanishing farfield radiation in momentum space. Most importantly, our experimental results confirm that the topological nature of the photonic BIC is perfectly transferred to the pol-BIC. This is evidenced with the observation of a polarization vortex in the farfield of polaritonic emission. Our results pave the way to engineer BIC physics of interacting bosons, as well as novel room temperature polaritonic devices.

I. INTRODUCTION

Bound state in the Continuum (BICs) are peculiar localized states that are forbidden to radiate despite lying in a continuum of propagating waves. Once regarded as an ‘exotic’ quantum mechanical effect¹, the origin of BICs is nowadays fully unravelled as a particular solution of wave equations, which has led to their exploitation in other fields where it is straightforwardly attributed to destructive interference mechanisms or symmetry mismatches². The most active playground of BIC physics is in contemporary Photonics³ since most of optoelectronic devices rely on resonances and their coupling mechanisms with environment. Indeed, the trapping of light through photonic BICs is a salient feature to enhance different light-matter interaction mechanisms, leading to various applications in microlasers^{4–8}, sensing⁹, optical switch⁷ and nonlinear optics^{10–13}. Moreover, on the fundamental side, photonic BICs in periodic lattices are pinned to singularities of farfield polarization vortex and can be considered as topological charges of non-Hermitian systems^{14–17}. This topological nature, together with modern technological feasibility to tailor photonic materials, makes photonic BICs a fruitful platform to engineer polarization singularities of open photonic systems^{5,18–20}.

Another prominent area of investigation in modern Optics is represented by exciton-polaritons, elementary excitations arising from the strong coupling regime between confined light and semiconductor excitons²¹. As hybridized eigenmodes, these bosonic quasiparticles inherit original features of both photonic resonances and excitonic ones. During the last decades, exciton-polaritons have become a standard platform to explore exotic phenomena of out-of-equilibrium Bose Einstein condensations²² and quantum fluid properties of electromagnetic fields²³, as well as novel concepts for all-optical devices. While most of the milestones of polaritonic physics have been achieved with excitonic material operating in cryogenic temperatures (~ 10 K), recent progress in material science has promoted many polaritonic demonstrations at room temperature with a wide variety of high bandgap semiconductors, ranging from GaN^{24,25}, ZnO²⁶, to organic semiconductors^{27,28} and transition metal dichalcogenide monolayers^{29,30}, as well as perovskite materials^{31–38}.

Very recently, the strong coupling regime between photonic BICs and excitonic resonances has been theoretically suggested,^{39–42} with two experimental demonstrations^{43,44}. The result of such a coupling is the formation of polariton-BICs (pol-BICs): hybrid excitations that are completely decoupled from the radiative continuum. This scenario is quite different from the text-book architecture in which the strong coupling regime is engineered by embedding quantum wells at the antinode positions of planar microcavities, which always exhibit substantial nonradiative losses. As state-of-the-

^{a)}Electronic mail: hai-son.nguyen@ec-lyon.fr

art, non-linear behaviors of pol-BICs⁴³ and the use of pol-BICs to trigger Bose-Einstein Condensation have been recently demonstrated⁴⁴. However, most of these demonstrations are conducted at cryogenic temperatures. Therefore, making pol-BICs with room temperature operation would be the next important step for the development of polaritonic devices based on BIC concepts.

Perovskite material has appeared in the last few years as the ideal alternative candidate to study exciton-polaritons at room temperature.⁴⁵ Nowadays, polaritonic Bose-Einstein condensation in the perovskite platform can be engineered to reproduce many features that have been up to now only evidenced in cryogenic GaAs-based polaritons.^{34,35,37,38} Moreover, the possibility to obtain high quality perovskite layers via solution-based methods opens feasible and low-cost approaches to fabricate perovskite metasurfaces. In this approach, the tailoring of the real part (i.e. frequency) of polaritonic energy-momentum dispersion has been experimentally demonstrated with sub-wavelength perovskite metasurface, in which linear, parabolic and multi-valley dispersion characteristics have been reported.³⁸ Most recently, it has been theoretically suggested that perovskite metasurfaces can be harnessed to engineer the imaginary part (i.e., losses) of the polaritonic energy-momentum dispersion at room temperature via BIC and Exceptional Point concepts.^{40,42}

In this work, we experimentally demonstrate the formation of pol-BICs in an excitonic metasurface made from hybrid 2D perovskites. The pol-BICs, revealed in both reflectivity, resonant scattering, and photoluminescence measurements, are robust at room temperature. They are originated from the strong coupling regime between a symmetry-protected BIC and the excitonic resonance of the perovskite material. Although the pol-BICs only exhibit finite quality factor, which is actually limited by the non-radiative losses from the excitonic component, they fully inherit the purely photonic BIC peculiar features: the decoupling from the radiative continuum, and the farfield emission vanishing at Γ point. Remarkably, the pol-BICs also inherit the topological nature of the purely photonic BICs. This is demonstrated through the observation of a polarization vortex in the farfield emission of pol-BIC modes.

II. RESULTS AND DISCUSSION

Our excitonic material is a 2D layered hybrid organic-inorganic perovskite, namely bi-(phenethylammonium) tetraiodoplumbate, known as PEPI, with chemical formula $(C_6H_5C_2H_4NH_3)_2PbI_4$. Thanks to the alternation between organic and inorganic monolayers (see Fig. 1b), PEPI thin films behave like a multi-quantum well structure where excitons are confined within inorganic monolayers. PEPI is one of the most widespread perovskite material for polaritonic applications, thanks to its giant exciton binding energy (\sim hundred meV at room temperature)⁴⁶. Here the fabrication of PEPI metasurface follows the same method previously reported (see Fig. 1c for a simplified sketch).³⁸ The PEPI solution is infiltrated inside air holes of pre-patterned silica backbone via spincoating, then followed by a thermal annealing to

form a square lattice of crystallized PEPI nano-pillars. The final sample is encapsulated with Poly-methyl methacrylate (PMMA) to protect PEPI against humidity.

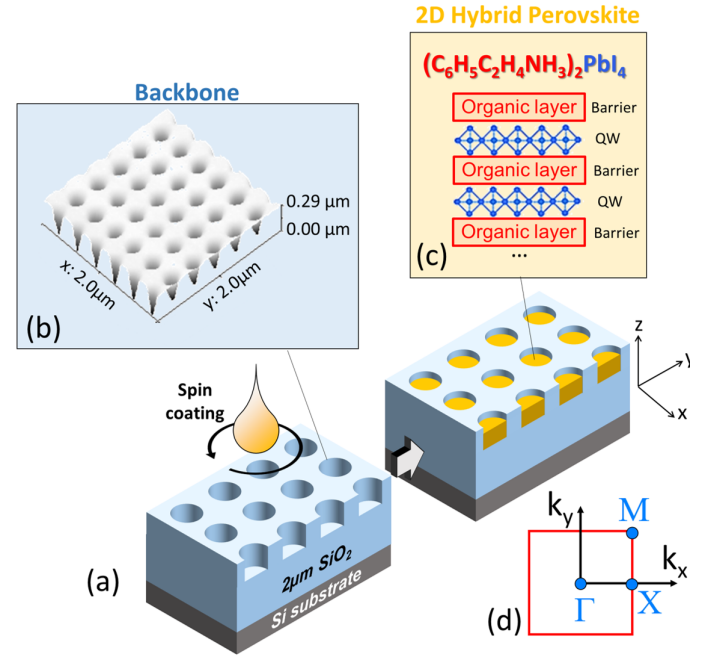


FIG. 1. a). Sketch of the fabrication method of the perovskite metasurface. The backbone consists of a $2\ \mu\text{m}$ -thick thermal SiO_2 on silicon substrate. It is pre-patterned into a square lattice of holes, with period $a = 330\ \text{nm}$, diameter $d = 132\ \text{nm}$ and depth $t_{\text{SiO}_2} = 150\ \text{nm}$. The crystallized perovskite layer has a total thickness $t_{\text{PEPI}} = 180\ \text{nm}$. Thus there is a residual $30\ \text{nm}$ -PEPI slab (not shown in the sketch). The final structure is encapsulated by $200\ \text{nm}$ -thick PMMA (not shown in the sketch). b) Atomic Force Microscopy (AFM) image of the photonic backbone. c) The layered structure of PEPI. d) The reciprocal space of the our metasurface with square Brillouin zone of size $2\pi/a$.

Our excitonic metasurface is designed so that the exciton energy ($E_X = 2.394\ \text{eV}$) is in the vicinity of the lowest Bloch resonances of the passive structure (PEPI is replaced by a dielectric material of constant refractive index $n = 2.4$). In Fig. 2a we report the energy-momentum dispersion and the corresponding quality factor (color-coded into the plot by points) of such Bloch resonances as calculated by Guided-Mode Expansion (GME) method,⁴⁷ generalized to deal with multilayered and partially etched dielectric materials.⁴⁸ The dispersion is calculated along ΓX direction (i.e. k_x , see Fig. 1d). Only modes with an odd parity with respect to mirror symmetry for reflection through the xz ($y = 0$) plane are shown in Fig. 2a (see supplementary material for the whole spectrum including even modes), which can be excited by transverse-electric polarized incident radiation. These results show that the lowest mode is a bright (low Q-factor) one at Γ point, while two singly-degenerate BICs are present at slightly higher energy, here denoted BIC_1 and BIC_2 . The theoretical electric field patterns of these two photonic BICs are reported in Fig. 2b,c, showing both E_x and E_y components, both in

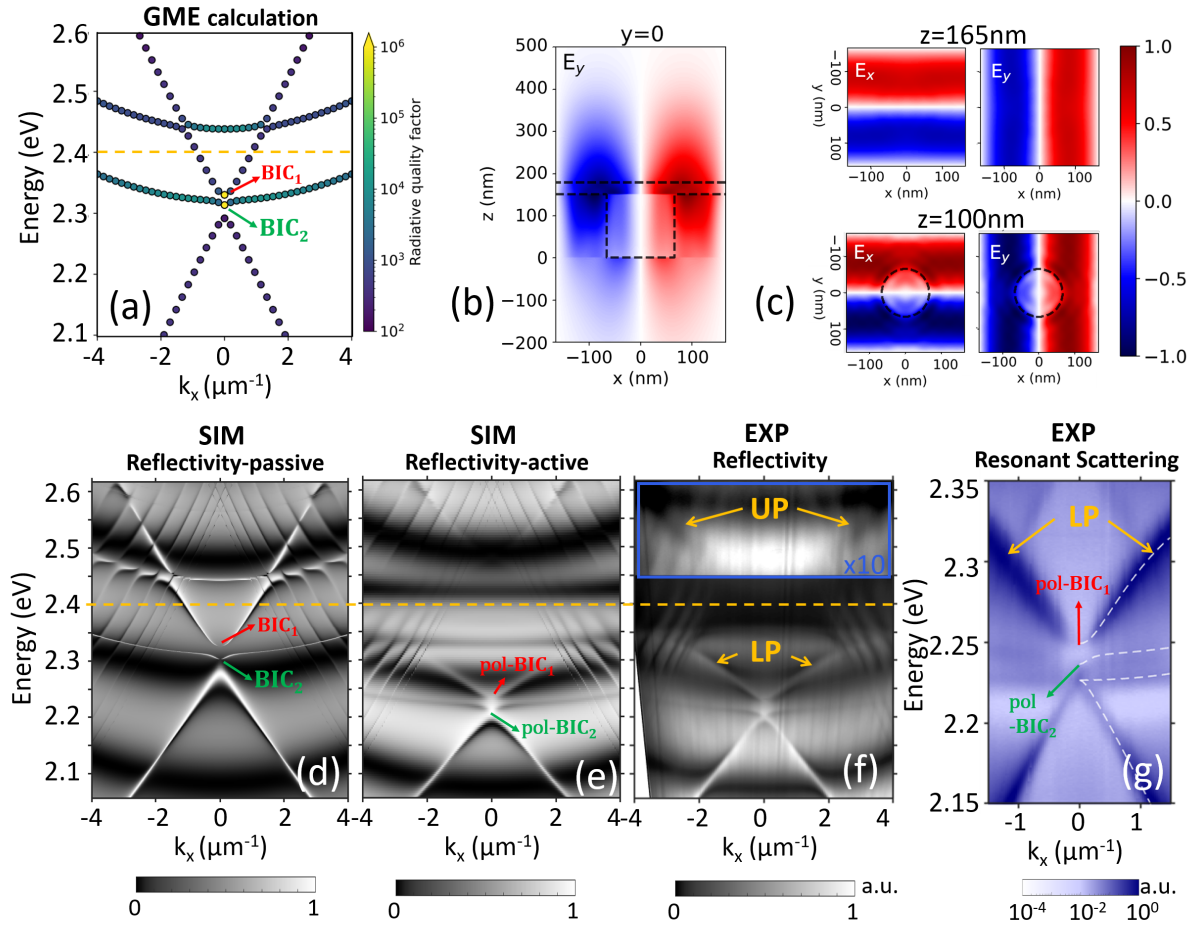


FIG. 2. (a) Energy-momentum dispersion calculated by GME for the passive metasurface by GME method for odd modes with respect to mirror symmetry for reflection against the xz plane (at $y = 0$); the Q-factor of each k_x -dependent mode is encoded in the color scale of each point (yellow corresponds to virtually infinite Q-factor, as determined from GME simulations). The dotted orange line indicates the exciton energy: $E_X = 2.394$ eV, and it is shown here for illustration purposes. (b) Spatial distribution of the electric field in the xz plane within a single unit cell of the square lattice, as obtained for the BIC_1 mode, and (b) corresponding cross sections in the xy plane for two different vertical coordinates, corresponding either to the patterned region (PEPI infiltrated hole) or the uniform PEPI region; we notice that the calculated field distribution for the BIC_2 is very similar. (d) Numerical simulations of the angle-resolved reflectivity spectra calculated for the passive structure (assuming the same parameters as the GME calculation), and (e) same simulation for the active structure (i.e., assuming a Lorentz oscillator model for the PEPI material, see methods), when excited by \uparrow (i.e. y) polarized light; also here the dashed line indicates the bare excitonic resonance of PEPI. (f) Experimental result of the angle-resolved reflectivity of the PEPI metasurface when excited by \uparrow polarized light. (g) Experimental result of the angle-resolved resonant scattering of the PEPI metasurface, zoomed in the vicinity of the two pol-BICs. The excitation is polarized along \nearrow (i.e. 45 degrees) and the detection is analysed along \nwarrow (i.e. -45 degrees). The dotted lines are guides to the eye to distinguish the 4 polaritonic modes.

vertical and planar cross sections. The odd parity of these spatial profiles for mirror symmetry through either xz or yz planes confirms that they are both symmetry-protected BICs, i.e., they are forbidden to couple to the radiative continuum due to their symmetry mismatch with radiative plane waves. As a result of numerical simulations using the Rigorous Coupled Wave Analysis (RCWA) method, Fig. 2d presents the calculated angle-resolved reflectivity of the passive structure when excited by \uparrow (i.e. y) polarized light, that is s-polarized (transverse electric, TE) with respect to the xz plane of in-

cidence. These results show very good agreement with the GME calculations for odd modes, we clearly distinguish the two BICs corresponding to the local vanishings of reflectivity resonances at $k_x = 0$. We also notice that only a singly degenerate leaky mode is shown in Fig. 2d with a maximum slightly below 2.3 eV, which matches the result in Fig. 2a. The other mode, degenerate in Γ , is of \leftrightarrow (i.e., x) polarization (clearly evidenced in the corresponding GME results for even modes and the corresponding RCWA simulations for p-polarized (transverse magnetic, TM) excitation with respect to

the xz incidence plane, shown in supplementary material).

We now investigate the coupling between PEPI excitons and the previous Bloch resonances, giving rise to polaritonic modes.⁴⁹ A home-built setup for Fourier spectroscopy is employed to study the excitonic metasurface via angle-resolved and spectral-resolved experiments. The experimental results of angle-resolved reflectivity measurements (Fig. 2f) and numerical ones from RCWA simulation (Fig. 2e) are in perfect agreement. The strong coupling regime is evidently demonstrated in both experimental and numerical results, by comparison with the simulations of the passive structures (i.e., without considering the excitonic response) in Fig. 2d. Indeed, all dispersion curves are strongly red-shifted from the bare exciton energy to form polaritonic branches. In particular, the anticrossings between the first lower polariton branch, here denoted LP, and the first upper polariton branch, here denoted UP, are clearly evidenced. The measured Rabi splitting is $\hbar\Omega \approx 200$ meV, which is in good agreement with previous reports on polaritons in PEPI metasurface,³⁸ as well as from the known expression for the radiation-matter coupling in confined systems in terms of the bulk material one⁵⁰, see also details in Methods.

Since the polaritonic modes inherit the symmetry properties of their photonic component, the first two LP branches possess the same odd parity at Γ point as the one of BIC₁ and BIC₂. Therefore, they must be symmetry-protected pol-BICs, denoted as pol-BIC₁ and pol-BIC₂, according to their photonic counterparts. To evidence their decoupling from the radiative electromagnetic continuum, a straightforward criterion is the vanishing of these resonances at Γ point, i.e. at normal incidence with respect to the metasurface. Although these vanishing resonances are hinted in Figs. 2e,f, it is a tricky observation because the reflectivity resonances corresponding to these guided modes have Fano-like profiles superimposed on a shallow Fabry-Perot modulation deriving from the $2\ \mu\text{m}$ -thick SiO₂.⁵¹ We get rid of such a background by employing resonant scattering measurements,⁵² in which the excitation and detection are in cross-polarization configuration (excitation in 45-degrees polarization direction, and analyzed in -45-degrees one). As shown in Fig. 2g, we observe all four polariton lower branches, corresponding to the four Bloch resonances previously discussed. Notably, the resonant scattering results feature both E_x and E_y polarized modes. Indeed, the leaky branch of high curvature of E_x polarization is observed in resonant scattering results, and not in reflectivity measurements of E_y polarization. Most importantly, as expected, the resonant scattering vanishes locally at the two pol-BICs.

The reflectivity and resonant scattering measurements show that the PEPI metasurface can host pol-BICs modes. To populate these polaritonic modes and study their farfield emission, we perform non-resonant pumping ($\lambda_{laser} = 400$ nm, 80 MHz, 50 ps) with the same Fourier spectroscopy setup. Angle-resolved photoluminescence results, shown in Fig. 3a, indicate that only the LP branch is efficiently populated while other modes (the UP and photonic-like bands at low energy) are either not observed or weakly populated. This observation is in good agreement with polaritonic behaviours in high bandgap materials for which the photoluminescence emission

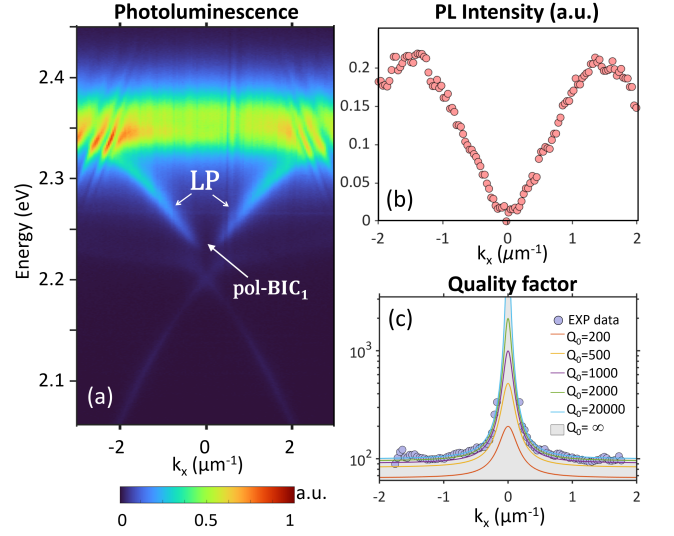


FIG. 3. (a) Angle-resolved photoluminescence results, analysed along \uparrow (i.e. y). (b) Angle-resolved emission intensity of the LP. (c) The quality factor of the LP extracted from the photoluminescence measurements. The blue circles are experimental data, the solid lines correspond to the model (1) with $Q_\infty = 95$, $\alpha = 5.9\ \mu\text{m}^2$ but using different values of Q_0 . The gray shading area corresponds to $Q_0 = \infty$.

is mainly visible for the first lower polariton branch. The farfield emission of the LP vanishes locally at $k_x = 0$ where the pol-BIC₁ resides. Such effect, already shown in Fig. 3a, is clearly evidenced in Fig. 3b where the photoluminescence intensity of the LP is tracked and reported. We note that the excitonic fraction of the pol-BIC₁ amounts to 35% as estimated from a simple model of two coupled oscillators, in which we take half of the Rabi splitting as the radiation-matter coupling energy (off-diagonal element in the 2 matrix, much larger than the oscillators linewidths) and the exciton-photon detuning estimated from the passive photonic BIC₁ mode (Fig. 2a) indicating that it is indeed an hybrid exciton-photon entity.

We now discuss on the use of a photonic BIC to enhance the quality factor of polaritonic modes. Since photonic BICs possess an ideally infinite quality factor, one may expect the same for pol-BICs. However, due to their hybrid exciton-photon nature, the quality factor of pol-BICs is balanced between the non-radiative losses of the excitonic component and the one from the photonic BIC⁴⁰. They are thus quasi-BICs, whose quality factor is limited by non-radiative losses. Moreover, the C_4 symmetry of the square-lattice imposes that the quality factor of photonic BICs decreases as k_x^2 at oblique angles.⁵ Therefore, within a small angular window close to normal incidence, the quality factor $Q(k_x)$ of the LP can be determined from a relatively simple law:

$$Q(k_x)^{-1} = Q_0^{-1} + \left(Q_\infty + \frac{\alpha}{k_x^2} \right)^{-1}, \quad (1)$$

in which Q_0 corresponds to the non-radiative losses originated from the excitonic component, Q_∞ corresponds to the radia-

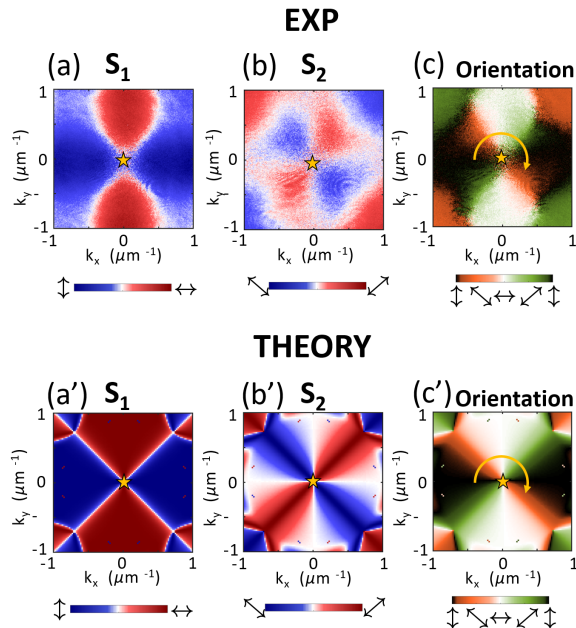


FIG. 4. Experimental results for the mapping of the Stokes parameters S_1 (a), S_2 (b), and the polarization orientation corresponding to pol-BIC₁ (c). Theoretically calculated S_1 (a'), S_2 (b'), and polarization orientation (c'), as obtained from GME simulations of the passive structure and corresponding to the BIC₁ Bloch mode of Fig. 2a.

tive losses of the photonic BIC at high oblique angles, and the coefficient α dictates the decreasing rate of the photonic BIC. Fig. 3b depicts the angular dependence of the quality factor of the LPB that are extracted from the photoluminescence spectra. The experimental data are nicely fitted by the model (1), with $Q_\infty = 95$, $\alpha = 5.9 \mu\text{m}^2$ and $Q_0 > 1000$. Therefore, our pol-BIC exhibits a quasi-BIC nature, indeed, having infinite radiative quality factor inherited from the photonic component, but a finite non-radiative one (> 1000) inherited from the excitonic component.

Despite being quasi-BICs with finite quality factor, pol-BICs preserve the nature of singularities in momentum space. This is due to a complete decoupling from the radiative continuum. As a consequence, every polaritonic branch that hosts a pol-BIC exhibits a polarization vortex around this singularity. In other words, pol-BICs fully inherit the topological behavior of their photonic components. To our knowledge, this fundamental property of pol-BICs has not been addressed in the literature, so far, either theoretically or experimentally. Here we investigate experimentally the polarization pattern of the LP branch in the vicinity of the pol-BIC₁. Figs. 4a,b present the measured Stokes parameters S_1 (Fig. 4a) and S_2 (Fig. 4b). These results evidence clearly the existence of a polarization singularity at Γ point. We note that the third Stokes parameter, S_3 (not shown here), is measured to be negligible, indicating that the ellipticity of the farfield polarization is also negligible. From the mapping of S_1 and S_2 , we can easily

extract the polarization orientation, ϕ , given by the relation $\tan\{2\phi\} = S_2/S_1$. The latter is reported in Fig. 4c, showing that ϕ decreases by an angle 2π when the Γ point is encircled. Therefore, the pol-BIC₁ is associated to a topological charge q , given by¹⁴:

$$q = \frac{1}{2\pi} \oint_C d\mathbf{k} \cdot \nabla_{\mathbf{k}} \phi = -1. \quad (2)$$

Finally, we theoretically verify that such topological nature of pol-BICs is indeed originated from the purely photonic BIC components. We report in Figs. 4a',b',c' the theoretically determined Stokes parameters and the corresponding polarization orientation of the photonic BIC₁, calculated from the GME results of the passive photonic structure (see Fig. 2a, and details in supplementary information). The striking similarity between these calculated patterns and the ones measured from pol-BIC₁ confirm that the photonic topological charge of this mode, $q = -1$, has been fully transferred to the polaritonic one.

III. CONCLUSION

In conclusion, we have experimentally demonstrated the formation of polariton BICs at room temperature in a perovskite-based resonant metasurface. As hybrid eigenmodes, these excitations inherit the non-radiative losses from the excitonic component, but at the same time preserve the topological nature of the purely photonic BIC. Our results suggest that excitonic metasurfaces are a promising platform to reveal and exploit polariton effects (such as nonlinearity, or interaction with magnetic field) with the engineering of polarization singularities. Indeed, one may think of using the polariton nonlinearity to control the merging/splitting of topological charges^{5,8}, or exploring the multi-bistable regimes of BIC physics^{10,12}. Moreover, this would pave the way to explore new regimes of polariton condensation and quantum fluids of light, in which the condensate is totally decoupled from the radiative continuum and is purely non-radiative.

IV. METHODS

A. Sample fabrication

The 2D structures were patterned using the laser interference lithography (LIL) technique. Substrates of $2 \mu\text{m}$ SiO₂/Si with size 1.5×1.5 cm were cleaned with acetone, ethanol, isopropanol then spincoated with photoresist MaN2403 at 5000 rpm in 30 sec then baked at 90°C in 1 min. These substrates were then put inside the LIL setup, exposed under laser $\lambda = 266$ nm with power 8 mW. Following this, we developed the samples in AZ-MIF 726 solution in 20 s. After LIL process, the patterns were formed on photoresist film and later transferred on SiO₂ using reactive ion etching (RIE) method. SiO₂ was etched by a gas combination of CHF₃/SF₆/CH₄ with respectively 16:6.2:2 sccm at pressure 20 mTorr with power set to 60 W. Followed by the fabrication of 2D patterns, PEPI

10% in DMF was deposited on the patterns by spincoating at 3000 rpm in 30 sec then annealed at 95°C in 90 sec. Last, we encapsulated PEPI from oxygen and humidity by spin coating PMMA resist on top of the whole structure at 5000 rpm in 30 sec and baking at 95°C in 5 min.

B. Fourier spectroscopy

The sample is excited by a halogen lamp (for reflectivity and resonant scattering measurements) or by non-resonant laser at 400 nm (for photoluminescence measurements) through a microscope objective ($\times 20$, NA=0.42). The scattered/emitter signal is collected via the same microscope objective and then is analysed in the momentum space by imaging the backfocal plane of the microscope objective onto the camera sensor. For dispersion measurement, the signal is first projected onto the entrance a spectrometer of which the output is coupled to the sensor of a CCD camera. For the farfield imaging, the signal is spectrally filtered by a band pass filter within 544 nm - 556 nm, and then projected onto the sensor of a sCMOS camera. Further information of the experimental setup is detailed in the Supplemental Material.

C. Polarization mapping

The mapping of Stokes parameters, $S_1(k_x, k_y)$, $S_2(k_x, k_y)$ and $S_3(k_x, k_y)$, is directly extracted from the photoluminescence farfield images, which are analysed in six different polarizations, respectively \leftrightarrow , \updownarrow , \nearrow , \nwarrow , \odot , \ominus . Then, the ellipticity, χ , is extracted from S_3 : $\sin\{2\chi\} = S_3$; the orientation, ϕ , is extracted from S_1 and S_2 as $\tan\{2\phi\} = S_2/S_1$.

D. Theoretical methods

The GME calculations have been performed by assuming an asymmetric planar waveguide with air (silica) as top (bottom) cladding, a core made of 200 nm thick PMMA (refractive index 1.49), 30 nm of unpatterned PEPI layer (index 2.41), and a square photonic lattice of 150 nm-thick circular PEPI pillars in a silica (index 1.48) backbone, lattice constant 330 nm, and pillar radius $r/a = 0.2$. The Stokes parameters are then calculated from the corresponding Bloch modes as²⁰ $c_x(k_x, k_y) = \hat{x} \cdot \langle \mathbf{u}(k_x, k_y) \rangle$ and $c_y(k_x, k_y) = \hat{y} \cdot \langle \mathbf{u}(k_x, k_y) \rangle$, where the Bloch functions \mathbf{u} are calculated within the meta-surface core (specifically, at half thickness of the patterned silica backbone), and the average $\langle \mathbf{u} \rangle$ is performed on the direct lattice unit cell. From these, we calculate $S_1 = |c_x|^2 - |c_y|^2$, $S_2 = 2\text{Re}\{c_x^* c_y\}$, and $S_3 = 2\text{Im}\{c_x^* c_y\}$. Finally, the Stokes parameters are normalized as $(S_1^2 + S_2^2 + S_3^2)^{1/2} = 1$.

The RCWA simulations of angular-resolved reflectivity have been performed with the S⁴ package provided by the Fan Group at the Stanford Electrical Engineering Department⁵³. The dielectric function of PEPI, used in RCWA simulations,

is given by:

$$\epsilon_{PEPI}(E) = n^2 + \frac{A_X}{E_X^2 - E^2 - i\gamma_X E} \quad (3)$$

where $n = 2.4$ is the refractive index of the passive structure, $A_X = 0.85 \text{ eV}^2$ is the oscillator strength of PEPI exciton, $E_X = 2.394 \text{ eV}$ is its energy and $\gamma_X = 30 \text{ meV}$ is its linewidth³⁸.

We notice that the Rabi coupling in polaritonic systems with confined excitons can be expressed in terms of the bulk value as

$$\hbar\omega_c \simeq \frac{\hbar\Omega}{2} = \hbar\omega_{\text{bulk}} \sqrt{\frac{L_w}{L_{\text{eff}}}} \quad (4)$$

in which $\hbar\omega_{\text{bulk}} = \sqrt{A_X}/n$, L_w is the thickness of the active layer (i.e., where the field is mostly intense), and L_{eff} is the effective extension length of the confined electric field. The latter quantities can be estimated from the field profile in Fig. 2b, i.e., $L_w \sim 30 \text{ nm}$, $L_{\text{eff}} \sim 300 \text{ nm}$. With these estimates we get $\hbar\Omega \simeq 240 \text{ meV}$, in good agreement with the experimentally determined value.

ACKNOWLEDGMENTS

The authors would like to thank the staff from the Nanolyon Technical Platform for helping and supporting in all nanofabrication processes. This work is partly supported by the French National Research Agency (ANR) under the project POPEYE (ANR-17-CE24-0020), project EMIPERO (ANR-18-CE24-0016) and the IDEXLYON from Université de Lyon, Scientific Breakthrough project TORE within the Programme Investissements d'Avenir (ANR-19-IDEX-0005). DS and DG acknowledge financial support from the Italian Ministry of Research (MIUR) through the PRIN 2017 project "Interacting photons in polariton circuits" (INPhoPOL).

¹J. Von Neumann and E. Wigner, "Über merkwürdige diskrete Eigenwerte," *Z. Phys* **30**, 465–497 (1929).

²C. W. Hsu, B. Zhen, A. D. Stone, J. D. Joannopoulos, and M. Soljačić, "Bound states in the continuum," *Nature Reviews Materials* **1**, 16048 (2016).

³S. I. Azzam and A. V. Kildishev, "Photonic bound states in the continuum: From basics to applications," *Advanced Optical Materials* **9**, 2001469 (2021), <https://onlinelibrary.wiley.com/doi/pdf/10.1002/adom.202001469>

⁴A. Kodigala, T. Lepetit, Q. Gu, B. Bahari, Y. Fainman, and B. Kanté, "Lasing action from photonic bound states in continuum," *Nature* **541**, 196–199 (2017).

⁵J. Jin, X. Yin, L. Ni, M. Soljačić, B. Zhen, and C. Peng, "Topologically enabled ultrahigh-Q guided resonances robust to out-of-plane scattering," *Nature* **574**, 501–504 (2019).

⁶M. Wu, S. T. Ha, S. Shendre, E. G. Durmusoglu, W.-K. Koh, D. R. Abujetas, J. A. Sánchez-Gil, R. Paniagua-Domínguez, H. V. Demir, and A. I. Kuznetsov, "Room-Temperature Lasing in Colloidal Nanoplatelets via Mie-Resonant Bound States in the Continuum," *Nano Letters* **20**, 6005–6011 (2020).

⁷C. Huang, C. Zhang, S. Xiao, Y. Wang, Y. Fan, Y. Liu, N. Zhang, G. Qu, H. Ji, J. Han, L. Ge, Y. Kivshar, and Q. Song, "Ultrafast control of vortex microlasers," *Science* **367**, 1018–1021 (2020).

⁸M.-S. Hwang, H.-C. Lee, K.-H. Kim, K.-Y. Jeong, S.-H. Kwon, K. Koshelev, Y. Kivshar, and H.-G. Park, "Ultralow-threshold laser using super-bound states in the continuum," *Nature Communications* **12**, 4135 (2021).

- ⁹S. Romano, G. Zito, S. Torino, G. Calafiore, E. Penzo, G. Coppola, S. Cabrini, I. Rendina, and V. Mocella, “Label-free sensing of ultralow-weight molecules with all-dielectric metasurfaces supporting bound states in the continuum,” *Photon. Res.* **6**, 726–733 (2018).
- ¹⁰S. D. Krasikov, A. A. Bogdanov, and I. V. Iorsh, “Nonlinear bound states in the continuum of a one-dimensional photonic crystal slab,” *Phys. Rev. B* **97**, 224309 (2018).
- ¹¹M. Minkov, D. Gerace, and S. Fan, “Doubly resonant $\chi^{(2)}$ nonlinear photonic crystal cavity based on a bound state in the continuum,” *Optica* **6**, 1039–1045 (2019).
- ¹²V. A. Zakharov and A. N. Poddubny, “Transverse magneto-optical kerr effect enhanced at the bound states in the continuum,” *Phys. Rev. A* **101**, 043848 (2020).
- ¹³J. Wang, M. Clementi, M. Minkov, A. Barone, J.-F. Carlin, N. Grandjean, D. Gerace, S. Fan, M. Galli, and R. Houdré, “Doubly resonant second-harmonic generation of a vortex beam from a bound state in the continuum,” *Optica* **7**, 1126–1132 (2020).
- ¹⁴B. Zhen, C. W. Hsu, L. Lu, A. D. Stone, and M. Soljačić, “Topological Nature of Optical Bound States in the Continuum,” *Physical Review Letters* **113**, 1–5 (2014).
- ¹⁵H. M. Doeleman, F. Monticone, W. den Hollander, A. Alù, and A. F. Koenderink, “Experimental observation of a polarization vortex at an optical bound state in the continuum,” *Nature Photonics* **12**, 397–401 (2018).
- ¹⁶Y. Zhang, A. Chen, W. Liu, C. W. Hsu, B. Wang, F. Guan, X. Liu, L. Shi, L. Lu, and J. Zi, “Observation of polarization vortices in momentum space,” *Phys. Rev. Lett.* **120**, 186103 (2018).
- ¹⁷B. Wang, W. Liu, M. Zhao, J. Wang, Y. Zhang, A. Chen, F. Guan, X. Liu, L. Shi, and J. Zi, “Generating optical vortex beams by momentum-space polarization vortices centred at bound states in the continuum,” *Nature Photonics* **14**, 623–628 (2020).
- ¹⁸X. Yin, J. Jin, M. Soljačić, C. Peng, and B. Zhen, “Observation of unidirectional bound states in the continuum enabled by topological defects,” (2019), [arXiv:1904.11464 \[physics.optics\]](https://arxiv.org/abs/1904.11464).
- ¹⁹W. Ye, Y. Gao, and J. Liu, “Singular points of polarizations in the momentum space of photonic crystal slabs,” *Phys. Rev. Lett.* **124**, 153904 (2020).
- ²⁰T. Yoda and M. Notomi, “Generation and annihilation of topologically protected bound states in the continuum and circularly polarized states by symmetry breaking,” *Phys. Rev. Lett.* **125**, 053902 (2020).
- ²¹C. Weisbuch, M. Nishioka, A. Ishikawa, and Y. Arakawa, “Observation of the coupled exciton-photon mode splitting in a semiconductor quantum microcavity,” *Phys. Rev. Lett.* **69**, 3314–3317 (1992).
- ²²J. Kasprzak, M. Richard, S. Kundermann, A. Baas, P. Jeambrun, J. M. J. Keeling, F. M. Marchetti, M. H. Szymańska, R. André, J. L. Staehli, V. Savona, P. B. Littlewood, B. Deveaud, and L. S. Dang, “Bose-Einstein condensation of exciton polaritons,” *Nature* **443**, 409–414 (2006).
- ²³I. Carusotto and C. Ciuti, “Quantum fluids of light,” *Rev. Mod. Phys.* **85**, 299–366 (2013).
- ²⁴S. Christopoulos, G. B. H. Von Högersthal, a. J. D. Grundy, P. G. Lagoudakis, a. V. Kavokin, J. J. Baumberg, G. Christmann, R. Butté, E. Feltn, J. F. Carlin, and N. Grandjean, “Room-temperature polariton lasing in semiconductor microcavities,” *Physical Review Letters* **98**, 1–4 (2007).
- ²⁵K. S. Daskalakis, P. S. Eldridge, G. Christmann, E. Trichas, R. Murray, E. Iliopoulos, E. Monroy, N. T. Pelekanos, J. J. Baumberg, and P. G. Savvidis, “All-dielectric GaN microcavity: Strong coupling and lasing at room temperature,” *Applied Physics Letters* **102** (2013), [10.1063/1.4795019](https://doi.org/10.1063/1.4795019).
- ²⁶H. Franke, C. Sturm, R. Schmidt-Grund, G. Wagner, and M. Grundmann, “Ballistic propagation of exciton polariton condensates in a ZnO-based microcavity,” *New Journal of Physics* **14**, 13037 (2012).
- ²⁷D. G. Lidzey, D. D. C. Bradley, M. S. Skolnick, T. Virgili, S. Walker, and D. M. Whittaker, “Strong exciton–photon coupling in an organic semiconductor microcavity,” *Nature* **395**, 53–55 (1998).
- ²⁸J. D. Plumbhof, T. Stöferle, L. Mai, U. Scherf, and R. F. Mahrt, “Room-temperature Bose–Einstein condensation of cavity exciton–polaritons in a polymer,” *Nature Materials* **13**, 247–252 (2014).
- ²⁹X. Liu, T. Galfsky, Z. Sun, F. Xia, E.-c. Lin, Y.-H. Lee, S. Kéna-Cohen, and V. M. Menon, “Strong light–matter coupling in two-dimensional atomic crystals,” *Nature Photonics* **9**, 30 (2014).
- ³⁰G. Grosso, “2D materials: Valley polaritons,” *Nature Photonics* **11**, 455–456 (2017).
- ³¹T. Fujita, Y. Sato, T. Kuitani, and T. Ishihara, “Tunable polariton absorption of distributed feedback microcavities at room temperature,” *Phys. Rev. B* **57**, 12428–12434 (1998).
- ³²N. Takada, T. Kamata, and D. D. C. Bradley, “Polariton emission from polysilane-based organic microcavities,” *Applied Physics Letters* **82**, 1812–1814 (2003).
- ³³G. Lanty, A. Bréhier, R. Parashkov, J.-S. Lauret, and E. Deleporte, “Strong exciton–photon coupling at room temperature in microcavities containing two-dimensional layered perovskite compounds,” *New Journal of Physics* **10**, 65007 (2008).
- ³⁴H. S. Nguyen, Z. Han, K. Abdel-Baki, X. Lafosse, A. Amo, J. S. Lauret, E. Deleporte, S. Bouchoule, and J. Bloch, “Quantum confinement of zero-dimensional hybrid organic-inorganic polaritons at room temperature,” *Applied Physics Letters* **104**, 1–5 (2014).
- ³⁵R. Su, C. Diederichs, J. Wang, T. C. H. Liew, J. Zhao, S. Liu, W. Xu, Z. Chen, and Q. Xiong, “Room-Temperature Polariton Lasing in All-Inorganic Perovskite Nanoplatelets,” *Nano Letters* **17**, 3982–3988 (2017).
- ³⁶A. Fieramosca, L. De Marco, M. Passoni, L. Polimeno, A. Rizzo, B. L. T. Rosa, G. Cruciani, L. Dominici, M. De Giorgi, G. Gigli, L. C. Andreani, D. Gerace, D. Ballarini, and D. Sanvitto, “Tunable out-of-plane excitons in 2d single-crystal perovskites,” *ACS Photonics* **5**, 4179–4185 (2018), <https://doi.org/10.1021/acsphotonics.8b00984>.
- ³⁷R. Su, S. Ghosh, J. Wang, S. Liu, C. Diederichs, T. C. H. Liew, and Q. Xiong, “Observation of exciton polariton condensation in a perovskite lattice at room temperature,” *Nature Physics* (2020), [10.1038/s41567-019-0764-5](https://doi.org/10.1038/s41567-019-0764-5).
- ³⁸N. H. M. Dang, D. Gerace, E. Drouard, G. Trippé-Allard, F. Lédée, R. Mazurczyk, E. Deleporte, C. Seassal, and H. S. Nguyen, “Tailoring Dispersion of Room-Temperature Exciton-Polaritons with Perovskite-Based Subwavelength Metasurfaces,” *Nano Letters* **20**, 2113–2119 (2020).
- ³⁹K. L. Koshelev, S. K. Sychev, Z. F. Sadrieva, A. A. Bogdanov, and I. V. Iorsh, “Strong coupling between excitons in transition metal dichalcogenides and optical bound states in the continuum,” *Phys. Rev. B* **98**, 161113 (2018).
- ⁴⁰L. Lu, Q. Le-Van, L. Ferrier, E. Drouard, C. Seassal, and H. S. Nguyen, “Engineering a light–matter strong coupling regime in perovskite-based plasmonic metasurface: quasi-bound state in the continuum and exceptional points,” *Photon. Res.* **8**, A91–A100 (2020).
- ⁴¹P. Xie, Z. Liang, T. Jia, D. Li, Y. Chen, P. Chang, H. Zhang, and W. Wang, “Strong coupling between excitons in a two-dimensional atomic crystal and quasibound states in the continuum in a two-dimensional all-dielectric asymmetric metasurface,” *Phys. Rev. B* **104**, 125446 (2021).
- ⁴²I. A. M. Al-Ani, K. As’Ham, L. Huang, A. E. Miroshnichenko, W. Lei, and H. T. Hattori, “Strong coupling of exciton and high-q mode in all-perovskite metasurfaces,” *Advanced Optical Materials* **n/a**, 2101120, <https://onlinelibrary.wiley.com/doi/pdf/10.1002/adom.202101120>.
- ⁴³V. Kravtsov, E. Khestanova, F. A. Benimetskiy, T. Ivanova, A. K. Samusev, I. S. Sinev, D. Pidgayko, A. M. Mozharov, I. S. Mukhin, M. S. Lohzkin, Y. V. Kapitonov, A. S. Brichkin, V. D. Kulakovskii, I. A. Shelykh, A. I. Tartakovskii, P. M. Walker, M. S. Skolnick, D. N. Krizhanovskii, and I. V. Iorsh, “Nonlinear polaritons in a monolayer semiconductor coupled to optical bound states in the continuum,” *Light: Science & Applications* **9**, 56 (2020).
- ⁴⁴V. Ardizzone, F. Riminucci, S. Zanotti, A. Gianfrate, D. G. Suarez-Forero, F. Todisco, M. D. Giorgi, D. Trypogeorgos, G. Gigli, H. S. Nguyen, K. Baldwin, L. Pfeiffer, D. Ballarini, D. Gerace, and D. Sanvitto, “Polariton bose-einstein condensate from a bound state in the continuum,” (2021), [arXiv:2105.09362 \[physics.optics\]](https://arxiv.org/abs/2105.09362).
- ⁴⁵R. Su, A. Fieramosca, Q. Zhang, H. S. Nguyen, E. Deleporte, Z. Chen, D. Sanvitto, T. C. H. Liew, and Q. Xiong, “Perovskite semiconductors for room-temperature exciton-polaritonic,” *Nature Materials* (2021), [10.1038/s41563-021-01035-x](https://doi.org/10.1038/s41563-021-01035-x).
- ⁴⁶K. Gauthron, J.-S. Lauret, L. Doyennette, G. Lanty, A. A. Chouéiry, S. J. Zhang, A. Brehier, L. Largeau, O. Manguin, J. Bloch, and E. Deleporte, “Optical spectroscopy of two-dimensional layered (C6H5C2H4-NH3)2-PbI4 perovskite,” *Opt. Express* **18**, 5912–5919 (2010).
- ⁴⁷L. C. Andreani and D. Gerace, “Photonic-crystal slabs with a triangular lattice of triangular holes investigated using a guided-mode expansion method,” *Phys. Rev. B* **73**, 235114 (2006).
- ⁴⁸M. Minkov, I. A. D. Williamson, L. C. Andreani, D. Gerace, B. Lou, A. Y.

- Song, T. W. Hughes, and S. Fan, "Inverse design of photonic crystals through automatic differentiation," *ACS Photonics* **7**, 1729–1741 (2020).
- ⁴⁹D. Gerace and L. C. Andreani, "Quantum theory of exciton-photon coupling in photonic crystal slabs with embedded quantum wells," *Phys. Rev. B* **75**, 235325 (2007).
- ⁵⁰A. Auffèves, D. Gerace, M. Richard, S. Portolan, M. França Santos, L. C. Kwek, and C. Miniatura, *Strong Light-Matter Coupling* (WORLD SCIENTIFIC, 2014) <https://www.worldscientific.com/doi/pdf/10.1142/8758>.
- ⁵¹M. Galli, D. Bajoni, M. Belotti, F. Paleari, M. Patrini, G. Guizzetti, D. Gerace, M. Agio, L. Andreani, D. Peyrade, and Y. Chen, "Measurement of photonic mode dispersion and linewidths in silicon-on-insulator photonic crystal slabs," *IEEE Journal on Selected Areas in Communications* **23**, 1402–1410 (2005).
- ⁵²M. W. McCutcheon, G. W. Rieger, I. W. Cheung, J. F. Young, D. Dalacu, S. Frédérick, P. J. Poole, G. C. Aers, and R. L. Williams, "Resonant scattering and second-harmonic spectroscopy of planar photonic crystal microcavities," *Applied Physics Letters* **87**, 221110 (2005), <https://doi.org/10.1063/1.2137898>.
- ⁵³V. Liu and S. Fan, "S4 : A free electromagnetic solver for layered periodic structures," *Computer Physics Communications* **183**, 2233–2244 (2012).
- ⁵⁴C. W. Hsu, B. Zhen, J. Lee, S.-I. Chua, S. G. Johnson, J. D. Joannopoulos, and M. Soljačić, "Observation of trapped light within the radiation continuum," *Nature* **499**, 188–191 (2013).

— Supplementary Material —

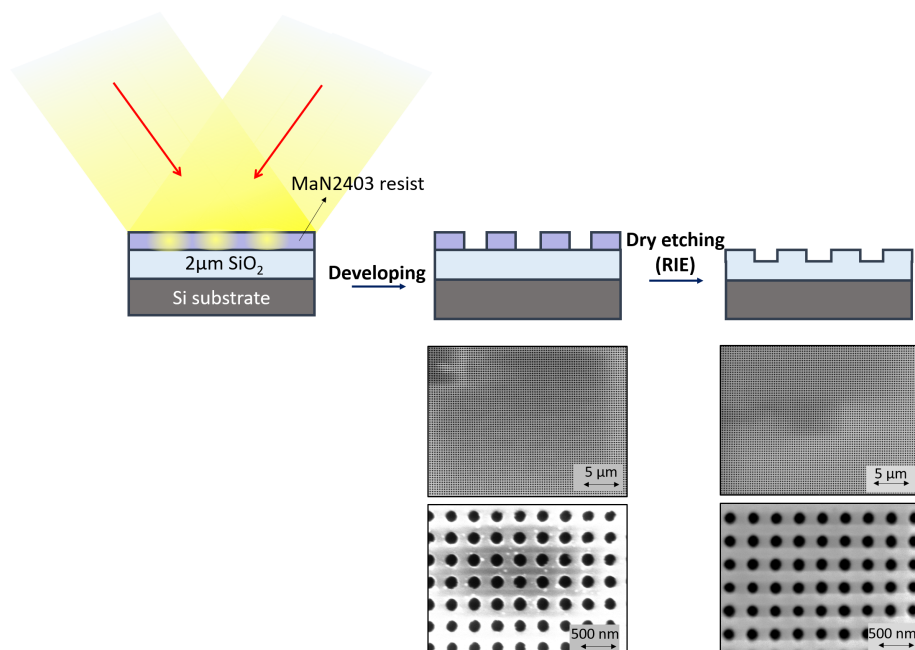


FIG. S1. LIL fabrication scheme of SiO₂ backbones and SEM images of samples before and after RIE process.

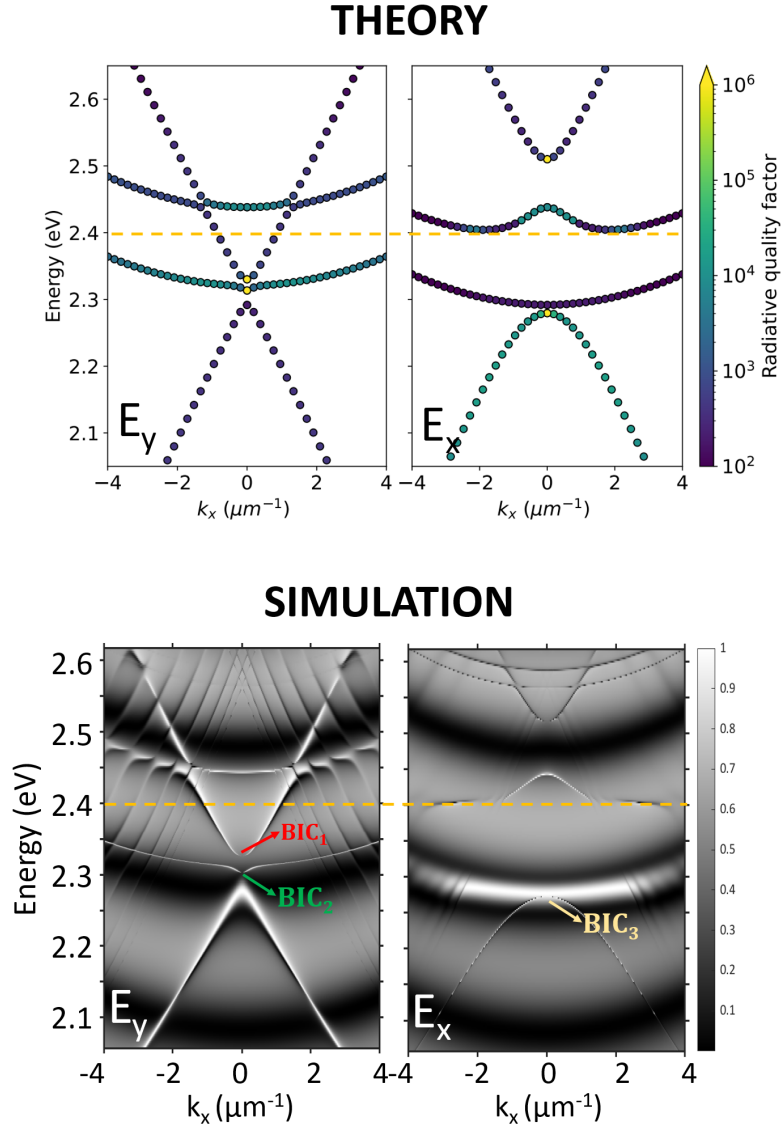


FIG. S2. Comparison between theoretical band structure of the passive PEPI metasurface, calculated by using the GME method (top panels) for both odd and even parity with respect to the xz plane, and the angle-resolved reflectivity spectra simulated by RCWA method (lower panels). Here, the considered structure is the passive one ($A_X = 0$). Interestingly, other than BIC_1 and BIC_2 in E_y polarization (i.e. odd parity about xz plane), other photonic BICs (here denoted BIC_3 and BIC_4) exist but they can be excited in E_x polarization (i.e., even parity about xz plane). However, they are far from the excitonic resonances (BIC_3 is at lower frequency and BIC_4 is at higher frequency), and their strong coupling with the excitonic resonance result in very photonic pol-BICs, and they are not populated at all in photoluminescence measurements.

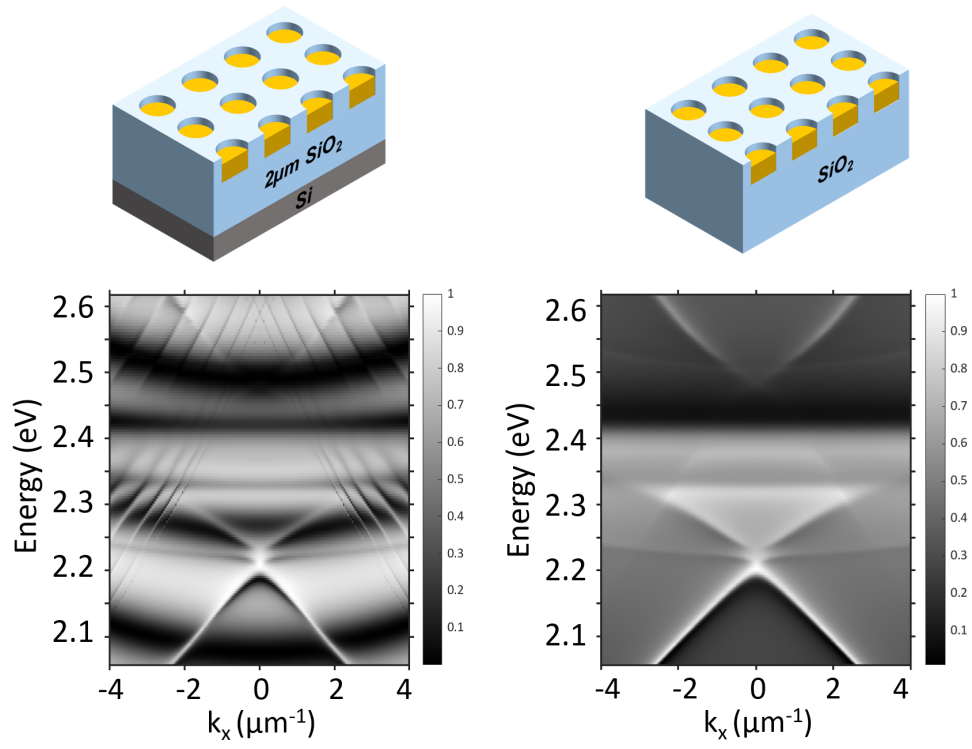


FIG. S3. Comparison between angle-resolved reflectivity spectra simulated by RCWA method of PEPI infiltrated inside $2\mu\text{m}$ SiO₂ on Si substrate (left panel) and inside pure SiO₂ substrate (right panel). These results allow to confirm which resonances come from the metasurface and not from the confinement within the SiO₂ layer.

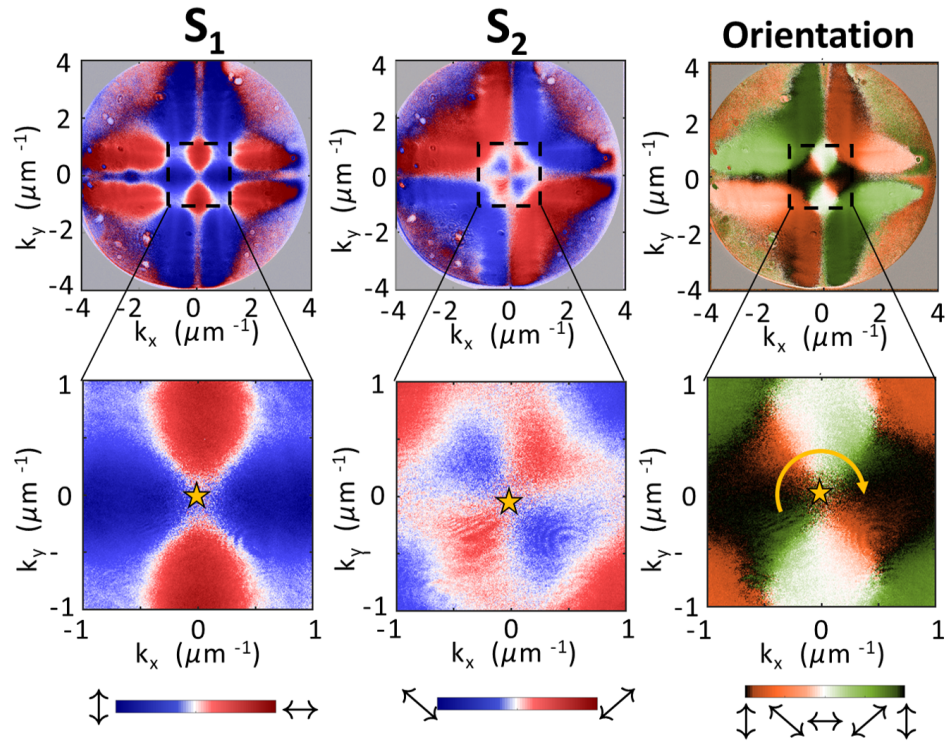


FIG. S4. Experimental results of the Stokes parameters, S_1 and S_2 , and the corresponding orientation angle, ϕ . Top panels: Unzoomed data. Lower panels: Zoomed data (as shown in the main text).

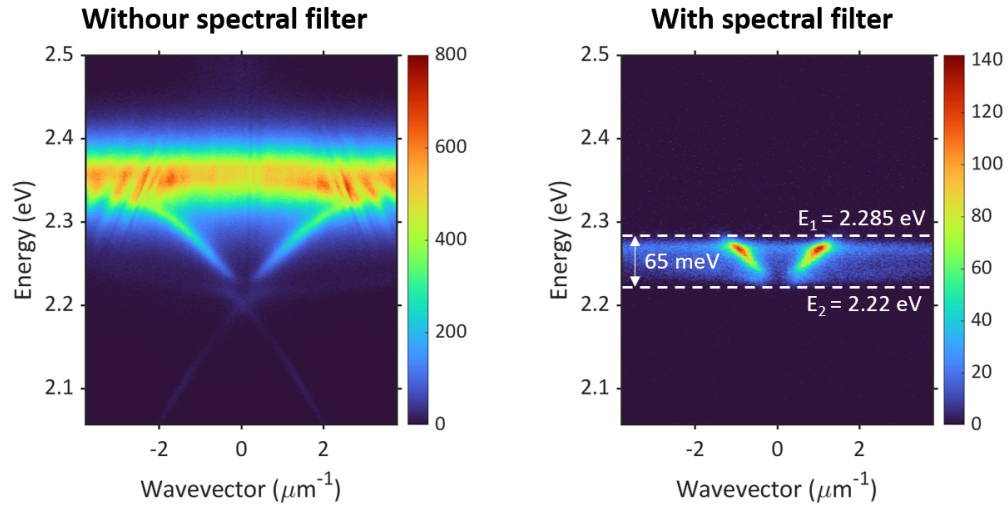


FIG. S5. Experimental angle-resolved photoluminescence dispersion with and without spectral filter. Here the spectral filter is the one used for mapping the Stoke parameters.

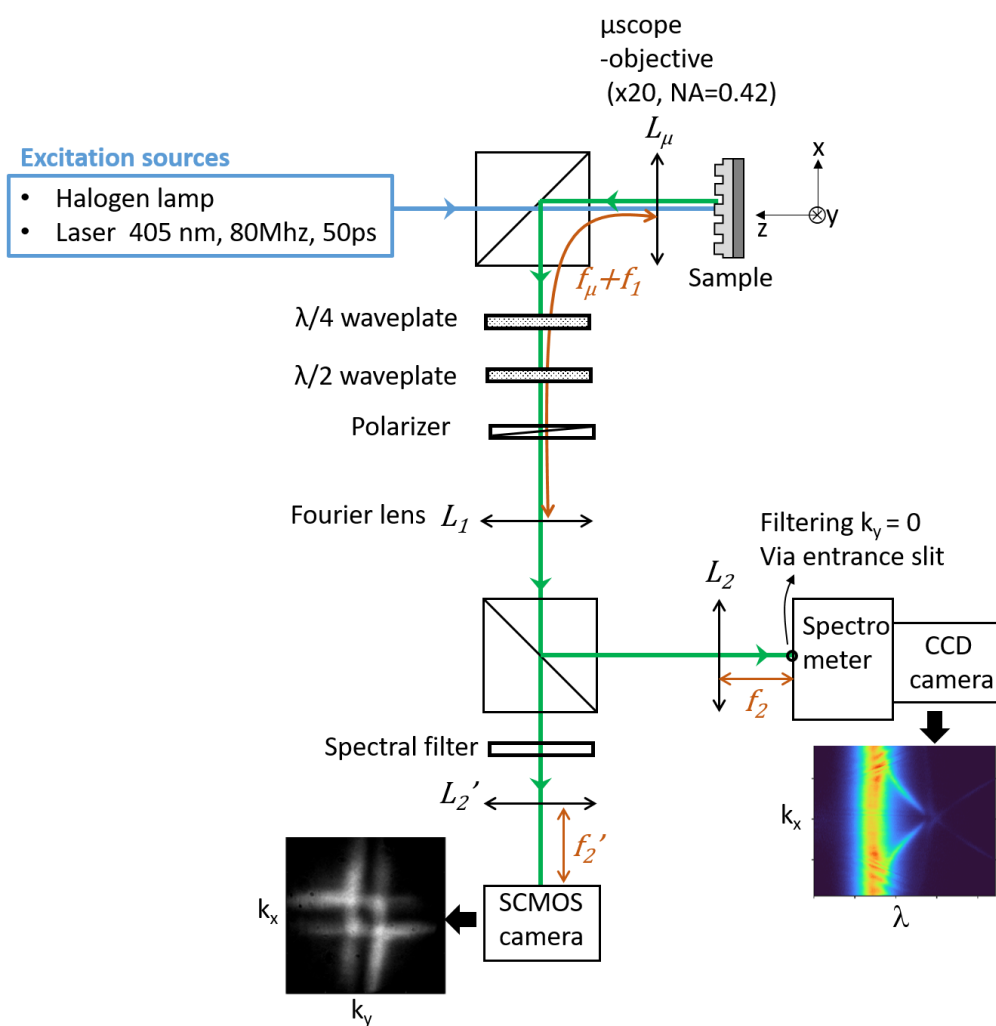


FIG. S6. Optical characterization setup for Fourier spectroscopy.